# Magnetization in quasiperiodic magnetic multilayers with biquadratic exchange coupling

C. G. Bezerra
*Departamento de Física, Universidade Federal do Rio Grande do Norte, 59072-970, Natal-RN, Brazil*

J. M. de Araújo
*Departamento de Ciências Naturais, Universidade Estadual do Rio Grande do Norte, 59610-210, Mossoró-RN, Brazil*

C. Chesman and E. L. Albuquerque[a)]
*Departamento de Física, Universidade Federal do Rio Grande do Norte, 59072-970, Natal-RN, Brazil*

(Received 17 July 2000; accepted for publication 20 November 2000)

A theoretical study of the magnetization curves of quasiperiodic magnetic multilayers is presented. We consider structures composed by ferromagnetic films (Fe) with interfilm exchange coupling provided by intervening nonferromagnetic layers (Cr). The theory is based on a realistic phenomenological model, which includes the following contributions to the free magnetic energy: Zeeman, cubic anisotropy, bilinear, and biquadratic exchange energies. The experimental parameters used here are based on experimental data recently reported, which contain sufficiently strong biquadratic exchange coupling. © *2001 American Institute of Physics.*
[DOI: 10.1063/1.1340600]

## I. INTRODUCTION

The study of the properties of magnetic multilayers has been one of the most investigated fields in the last decade. The understanding of a number of intriguing results became an exciting challenge from both a theoretical and experimental point of view. In their pioneer work, Grünberg and collaborators[1] reported evidence of an antiferromagnetic bilinear exchange coupling in Fe/Cr/Fe structures. After that, Baibich *et al.*[2] noticed a sudden fall in the electrical resistance of Fe/Cr magnetic multilayers when an external magnetic field was applied. The effect was so striking that it was called giant magnetoresistance, and recently it has been widely considered for applications in information storage technology.[3] Through magnetoresistance measurements, Parkin *et al.*[4] observed an oscillatory behavior of the exchange coupling in magnetic metallic multilayers as a function of the nonmagnetic spacer thickness. This work was seminal to a number of experimental studies on Fe/Cr/Fe structures with different nonmagnetic spacer thickness. Later on, in 1991, Rührig *et al.*[5] showed evidence of a noncolinear alignment (90°) between ferromagnetic layers in Fe/Cr magnetic multilayers, for nonmagnetic spacer thickness, where the bilinear exchange coupling was small. This behavior could not be explained considering only the usual bilinear exchange coupling in the free magnetic energy. In fact, the inclusion of a biquadratic exchange term in the free magnetic energy of the system allows the stabilization of noncolinear alignments. Until recently, it was found that the biquadratic exchange coupling was too small when compared to the bilinear exchange coupling. However, Azevedo and co-workers[6–8] presented a number of experimental results in Fe/Cr/Fe samples which show the biquadratic exchange coupling comparable to the bilinear exchange coupling. Therefore, the biquadratic coupling can play a remarkable role in the properties of magnetic multilayers.

On the other hand, from an experimental point of view, due to the rapid development of the crystal growth techniques, it is now possible to tailor a wide class of magnetic multilayers, whose film thickness is extremely well controlled. As a consequence, there are magnetic phases and properties which are not shared by the constituent materials.

It is known that magnetic properties can depend strongly on the stacking pattern of the layers. Under this aspect, the physical properties of a class of artificial material, the so-called quasiperiodic structures recently became an attractive field of research. Quasiperiodic structures, which can be idealized as the experimental realization of a one-dimensional quasicrystal, are composed by the superposition of two (or more) building blocks that are arranged in a desired manner. They can be defined as an intermediate state between an ordered system (a periodic crystal) and a disordered one (an amorphous solid).[9,10] One of the most interesting features of these systems is that the long range correlations, induced by the construction of the systems, are reflected in their various spectra. In fact, many physical properties of quasiperiodic systems have been studied such as light propagation,[11] phonons,[12] electronic transmission,[13] polaritons,[14] and magnons.[15] In all of these situations, despite the diversity of the systems a common feature is present, namely, a fractal spectra of energy, which can be considered as their basic signature.[16,17] However, only very recently were efforts taken towards the understanding of the properties of quasiperiodic magnetic multilayers.[15,18]

The main aim of this article is a contribution to the understanding of the effects of the quasiperiodic arrangement on the magnetization curves in magnetic multilayers. We are interested in magnetic phases and alignments that are only

a)Author to whom correspondence should be addressed; electronic mail: ela@dfte.ufrn.br

 

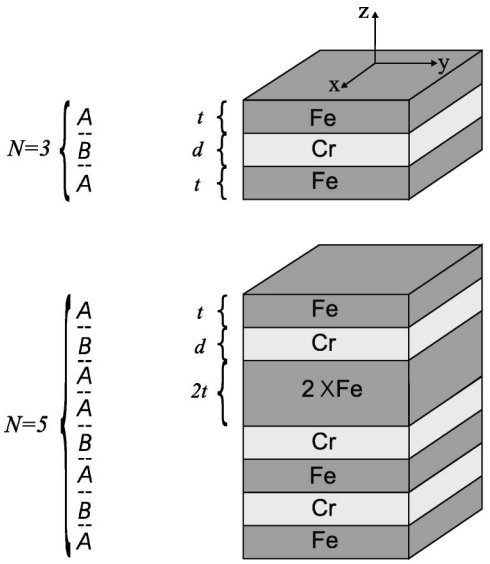


FIG. 1. The third and fifth Fibonacci generations and their magnetic counterpart.

due to the quasiperiodicity of the system. We have studied Fe/Cr(100) structures which follow a Fibonacci and a double period or *generalized Fibonacci* quasiperiodic sequences.

The layout of the article is as follows: In Sec. II we discuss the physical model used here, with emphasis in the description of the quasiperiodic sequences. In Sec. III we define the contributions to the magnetic energy. The numerical methods, used to obtain the equilibrium configuration, are described in Sec. IV. In Sec. V, the results are presented and discussed. Finally, we draw the conclusions in Sec. VI.

## II. PHYSICAL MODEL

A quasiperiodic structure can be experimentally constructed juxtaposing two building blocks (or, as considered here, building layers) following a given quasiperiodic sequence. We choose Fe as the building layer associated with the letter *A*, and Cr as the building layer associated with the letter *B* (see Fig. 1). Therefore, we only take into account the generation of sequences that start and finish with an Fe building layer, which means an even number of Fe layers, to guarantee a real magnetic counterpart. In this way we also avoid the intriguing behavior found when even and odd numbers of Fe layers are considered.[19] In this article we have considered two quasiperiodic sequences, namely, the Fibonacci and the double period sequences.

### A. The Fibonacci magnetic multilayers

The $N$th generation of the Fibonacci sequence can be determined appending the $N-2$ generation to the $N-1$ one, i.e., $S_N=S_{N-1}S_{N-2}$ $(N\geqslant 2)$. This algorithm construction requires initial conditions which are chosen to be $S_0=B$ and $S_1=A$. The Fibonacci generations can also be alternatively obtained by an iterative process from the substitution rules (or inflation rules), $A\rightarrow AB$, $B\rightarrow A$. The Fibonacci generations are

$$S_0=[B],\ S_1=[A],\ S_2=[AB],\ S_3=[ABA],\ \text{etc.}$$

In a given generation $S_N$, the total number of letters is given by the Fibonacci number $F_N$, which is obtained by the relation $F_N=F_{N-1}+F_{N-2}$, with $F_0=F_1=1$. Also, $F_{N-1}$ and $F_{N-2}$ are the number of letters *A* and *B*, respectively. As the generation order increases $(N\gg 1)$, the ratio $F_N/F_{N-1}$ approach to $\tau=(1+\sqrt{5})/2$, an irrational number which is known as the golden mean. It is also possible to obtain the number of letters *A* and *B* for a given generation by the substitution matrix of the Fibonacci sequence $\mathbf{M_F}$ from,[20]

$$\begin{bmatrix} n_A^{N+1} \\ n_B^{N+1} \end{bmatrix} = \mathbf{M_F} \begin{bmatrix} n_A^{N} \\ n_B^{N} \end{bmatrix}. \tag{1}$$

Here $(n_A^{N+1},n_B^{N+1})$ are the number of letters *A* and *B* in the $(N+1)th$ generation, and $(n_A^N,n_B^N)$ are the number of letters *A* and *B* in the $Nth$ generation. The explicit form of the substitution matrix for the Fibonacci sequence is,

$$\mathbf{M_F}=\begin{bmatrix} 1 & 1 \\ 1 & 0 \end{bmatrix}, \tag{2}$$

whose first eigenvalue $\lambda$ is the golden mean $\tau$.

In Fig. 1, we show the third and fifth Fibonacci generations and their magnetic counterparts. Note that the third Fibonacci generation corresponds to a trilayer Fe/Cr/Fe, and in the fifth Fibonacci generation there is a double Fe layer. It is easy to show that the Fibonacci magnetic multilayers, for any generation, are composed by single Cr layers, single Fe layers, and double Fe layers. The number of Fe single layers is $1+F_{N-2}$, the number of Fe double layers is $-1+F_{N-1}-F_{N-2}$ and the number of Cr layers is $F_{N-2}$. It should be observed that only odd Fibonacci generations have a magnetic counterpart (they start and finish with an Fe building layer).

### B. The double period magnetic multilayers

The $N$th generation of the double period sequence can be obtained from the relations,

$$S_N=S_{N-1}S_{N-1}^{\dagger}, \tag{3}$$

with

$$S_N^{\dagger}=S_{N-1}S_{N-1}(N\geqslant 2), \tag{4}$$

The initial conditions are $S_0=Ae$ $S_1=AB$. We can, alternatively, use the substitution rules $A\rightarrow AB$, $B\rightarrow AA$. The double period generations are

$$S_0=[A],\ S_1=[AB],\ S_2=[ABAA],\ \text{etc.}$$

In a given generation $S_N$, the total number of letters is $2^N$, and the number of letters *A* and *B* for consecutive generations can be related by the substitution matrix of the double period sequence $\mathbf{M_{dp}}$, i.e.,[20]

$$\begin{bmatrix} n_A^{N+1} \\ n_B^{N+1} \end{bmatrix} = \mathbf{M_{dp}} \begin{bmatrix} n_A^{N} \\ n_B^{N} \end{bmatrix}. \tag{5}$$

Here $(n_A^{N+1},n_B^{N+1})$ are the number of letters *A* and *B* in the $(N+1)th$ generation, and $(n_A^N,n_B^N)$ are the number of letters

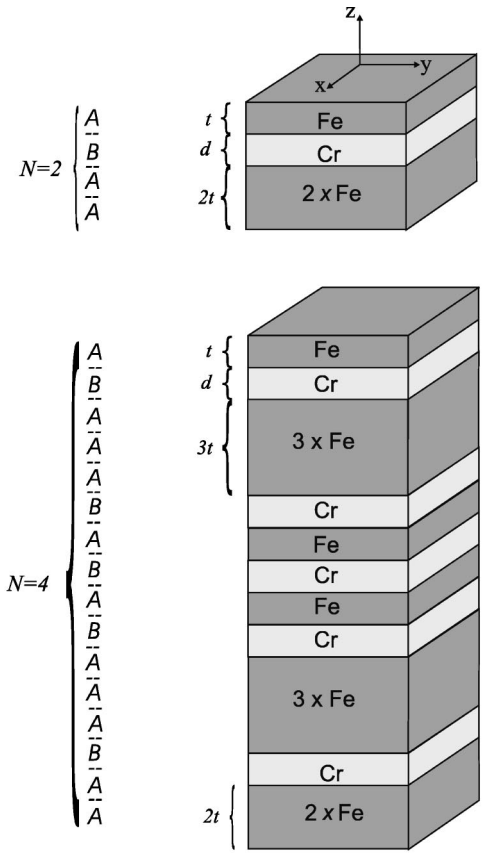


FIG. 2. Same as Fig. 1 for the second and fourth double period generations.

$A$ and $B$ in the $Nth$ generation. As the generation number increases ($N \gg 1$), the ratio between the number of letters $A$ and $B$ tends to 2. The explicit form of the substitution matrix for the double period sequence is

$$\mathbf{M_F} = \begin{bmatrix} 1 & 1 \\ 2 & 1 \end{bmatrix}. \tag{6}$$

In Fig. 2 we show the second and fourth double period generations and their magnetic counterparts. The double period magnetic multilayers are composed by single Fe layers, double Fe layers, triple Fe layers, and single Cr layers. It should be observed that, contrary to the Fibonacci case, only even double period generations have a magnetic counterpart.

## III. MAGNETIC ENERGY

We consider magnetic multilayers whose constituents are Fe ferromagnetic films, separated by Cr nonmagnetic films. We take the $xy$ plane as the film plane and the $z$ axis as the growth direction. We consider that the magnetic films are uniformly magnetized and that they behave as monodomains. We also consider that they do not present dynamical excitations and that the very strong demagnetization field, generates by tipping the magnetization out of the plane, will suppress any tendency for the magnetization to tilt out of plane. Therefore, the degrees of freedom of the magnetizations are restricted to the $xy$ plane. The interfilm exchange couplings between the ferromagnetic films are weak when compared to the strong exchange couplings between spins within a given ferromagnetic film. Therefore, we can represent the ferromagnetic films as classical magnetizations $\vec{M}$, composed by the real spins within the films, which are strongly coupled by the intrafilm exchange coupling. These classical magnetizations interact through the interfilm exchange coupling and they can present some anisotropy depending on the structure studied. It should be noted that this system is isomorphous to a one-dimensional chain of classical spins.

The global behavior of this system is well described by a realistic phenomenological theory in terms of the free magnetic energy,[7] i.e.,

$$E_T = E_z + E_{\rm ca} + E_{\rm bl} + E_{\rm bq}. \tag{7}$$

Here $E_z$ is the Zeeman energy (between the ferromagnetic films and the external applied magnetic field), $E_{\rm ca}$ is the cubic crystalline anisotropy energy (which we consider present in the ferromagnetic films) and $E_{\rm bl}$ and $E_{\rm bq}$ are the bilinear and the biquadratic exchange coupling energies (between the ferromagnetic films), respectively.

The explicit form of the free magnetic energy can be written as

$$\begin{aligned} E_T = & -\sum_{i=1}^{n} t_i \vec{M}_i \cdot \vec{H} + \sum_{i=1}^{n} \frac{t_i K_{\rm ca}}{|M_i|^4} \\ & \times (M_{ix}^2 M_{iy}^2 + M_{ix}^2 M_{iz}^2 + M_{iy}^2 M_{iz}^2) \\ & - \sum_{i=1}^{n-1} J_{\rm bl} \frac{\vec{M}_i \cdot \vec{M}_{i+1}}{|\vec{M}_i||\vec{M}_{i+1}|} + \sum_{i=1}^{n-1} J_{\rm bq} \frac{(\vec{M}_i \cdot \vec{M}_{i+1})^2}{|\vec{M}_i|^2 |\vec{M}_{i+1}|^2}. \end{aligned} \tag{8}$$

Here, $\vec{H}$ is the external magnetic field which is applied in the film plane, $t_i$ is the thickness of the $i$th Fe layer, $\vec{M}_i$ is the classical magnetization of the $i$th Fe layer, and $K_{\rm ca}$ is the cubic anisotropy constant. Also, $J_{\rm bl}$ and $J_{\rm bq}$ are the bilinear and the biquadratic exchange couplings, respectively. This expression, after a tedious but straight calculation, takes the form,

$$\begin{aligned} E_T = & \sum_{i=1}^{n} \left\{ -t_i M_i H \cos(\theta_i - \theta_H) + \frac{1}{4} t_i K_{\rm ca} \sin^2(2\theta_i) \right\} \\ & + \sum_{i=1}^{n-1} \{ -J_{\rm bl} \cos(\theta_i - \theta_{i+1}) + J_{\rm bq} \cos^2(\theta_i - \theta_{i+1}) \}. \end{aligned} \tag{9}$$

Here $\theta_i$ is the angular orientation of the magnetization of the $i$th Fe layer and $\theta_H$ is the angular orientation of the magnetic field. From this point we consider $\theta_H = 0$, which means that the magnetic field is applied along the easy axis. It is usual to write the total free magnetic energy in terms of experimental parameters, like

$$H_{\rm ca} = \frac{2K_{\rm ca}}{M_S}, \tag{10}$$

$$H_{\rm bl} = \frac{J_{\rm bl}}{tM_S}, \tag{11}$$

$$H_{\rm bq} = \frac{J_{\rm bq}}{tM_S}. \tag{12}$$

In this way we obtain a final expression for the free magnetic energy per unit area

$$\frac{E_T}{tM_S}=\sum_{i=1}^{n}(t_i/t)\left\{-H_0\cos(\theta_i)+\frac{1}{8}H_{\rm ca}\sin^2(2\theta_i)\right\}+\sum_{i=1}^{n-1}\{-H_{\rm bl}\cos(\theta_i-\theta_{i+1})+H_{\rm bq}\cos^2(\theta_i-\theta_{i+1})\}. \quad (13)$$

Here $t$ is the thickness of a single Fe layer which is considered to be the basic tile, $M_i$ is assumed to be equal to $M_S$ (the saturation magnetization), and $H_{\rm ca}$ is the cubic anisotropy field which turns the (100) direction an easy direction. $H_{\rm bl}$ is the bilinear exchange coupling field which favors antiferromagnetic alignment when negative, and ferromagnetic alignment when positive. $H_{\rm bq}$ is the biquadratic exchange coupling field which is experimentally found to be positive and favors a noncolinear alignment (90°) between two adjacent magnetizations.

Once the free magnetic energy is determined, we can calculate the equilibrium configuration for specific values of the experimental parameters as a function of the external applied field. In simple situations, the equilibrium configuration can be analytically obtained by equating to zero the derivatives of the magnetic energy with respect to the angle $\theta$. However, in most cases this leads to transcendental equations which can not be analytically solved. From a numerical point of view, many methods have been proposed to calculate the equilibrium positions of the magnetizations. In the next section we describe the methods used in this article.

## IV. NUMERICAL METHODS

In this section we want to find the global minimum of the cost function

$$E_T=E_T(\theta_1,\theta_2,\ldots,\theta_n), \quad (14)$$

where $\theta_n$ can assume values in the range $[0,2\pi]$ and it defines a $n$-dimensional space. When the dimension of this space is high, the cost function has a rough surface, i.e., there are many local minima which make this difficult to find the global minimum. There are many numerical methods to solve this problem.[21] In our specific case two methods were successfully used, namely, simulated annealing and the so-called gradient method.

### A. Simulated annealing method

Introduced by Kirkpatrick *et al.*[22] simulated annealing comes from the fact that the heating (annealing) and slowly cooling a metal, brings it into a more uniformed crystalline state, which is believed to be the state where the free energy of bulk matter takes its global minimum. The role played by the temperature is to allow the configurations to reach higher energy states with probability given by Boltzmann's exponential law. Then they can overcome energy barriers that would otherwise force them into local minima. In general, a simulated annealing technique can be written as follows:

(i) Choose an initial point in parameter space, corresponding to an initial configuration $\{\theta\}_j$, and calculate the associated energy $E_j$.
(ii) Choose a second point in parameter space, corresponding to a second configuration $\{\theta\}_{j+1}$, and calculate the associated energy $E_{j+1}$.
(iii) If $\Delta E=E_{j+1}-E_j<0$, $\{\theta\}_{j+1}$ is the new configuration of the system.
(iv) If $\Delta E\geqslant 0$, we define the probability $p=\exp(-\Delta E/k_BT)$ and choose a random number $0\leqslant x\leqslant 1$. If $x\geqslant p$, $\{\theta\}_{j+1}$ is the new configuration of the system. Otherwise, $\{\theta\}_j$ is maintained as the configuration of the system.
(v) This procedure is executed again and again until the equilibrium is reached.

### B. The gradient method

The second method that we have used was the so-called gradient method.[23] This method is based on the directional derivative of the cost function (the magnetic energy) in the search of its global minimum.[23] In this way, we need to calculate the gradient of $E_T$ with relation to the set $\{\theta\}$

$$\vec{\nabla}E_T=\sum_{i=1}^{n}\frac{\partial E_T}{\partial\theta_i}\hat{\theta}_i. \quad (15)$$

From this relation we execute the following algorithm to find the equilibrium configuration,

(i) We generate a configuration in the parameter space $\{\theta\}_j$ from which we calculate the associated energy $E_j$ and the gradient of the cost function.
(ii) A second point in the parameter space is generated by $\{\theta\}_{j+1}=\{\theta\}_j-\alpha\vec{\nabla}E_T$. Here $\alpha$ controls the size of the displacement in the direction $-\vec{\nabla}E_T$.
(iii) The energy of the second point is calculated and if $E_{j+1}>E_j$, the parameter $\alpha$ (the size of the displacement) is divided by two and we go back to (ii). Otherwise, we instead generate a new configuration from $\{\theta\}_{j+1}$.

In the last step the reduction of $\alpha$ is limited by the precision value required for $\epsilon$. This limit is reached when $|\alpha\vec{\nabla}E_T|<\epsilon$.

We have used the two methods discussed above to obtain the equilibrium positions of the magnetizations. Each method was applied for each value of the applied magnetic field and for each set of experimental parameters. We choose the configuration with the lowest energy furnished by both methods as the equilibrium configuration.

## V. NUMERICAL RESULTS

In this section we present the numerical results obtained for the magnetization curves of quasiperiodic magnetic multilayers. In all situations we have considered the cubic anisotropy effective field $H_{\rm ca}=0.5$ kOe which corresponds to Fe(100) with $t>30$ Å. In our calculations we have used two sets of experimental values for the bilinear and biquadratic

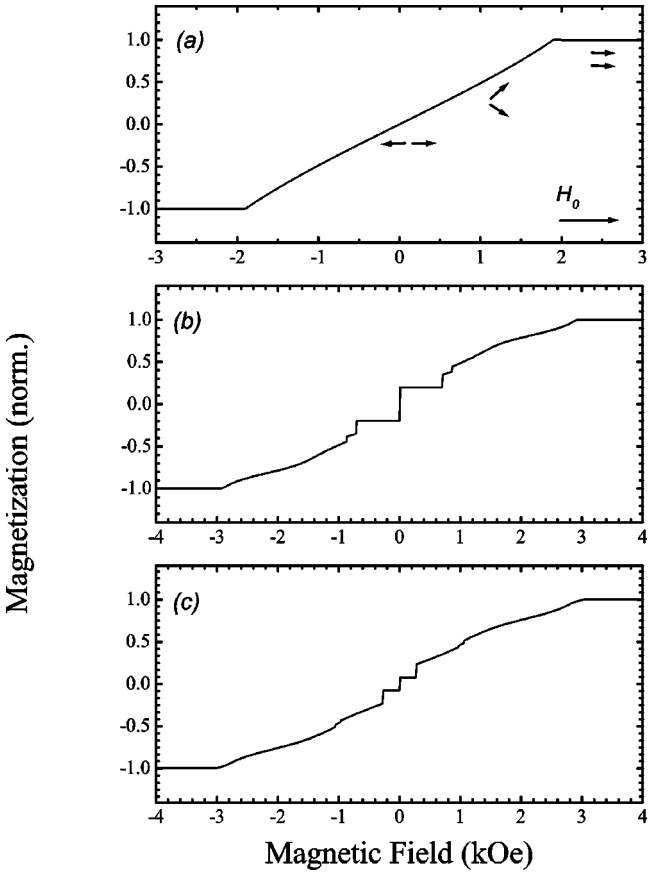


FIG. 3. Magnetization vs applied field for the third (a), fifth (b), and seventh (c) Fibonacci generations with $|H_{bq}|/|H_{bl}|=0.10$, corresponding to a realistic sample whose Cr thickness is about 10 Å. We have considered the cubic anisotropy effective field $H_{ca}=0.5$ kOe, which corresponds to Fe(100) with $t>30$ Å.

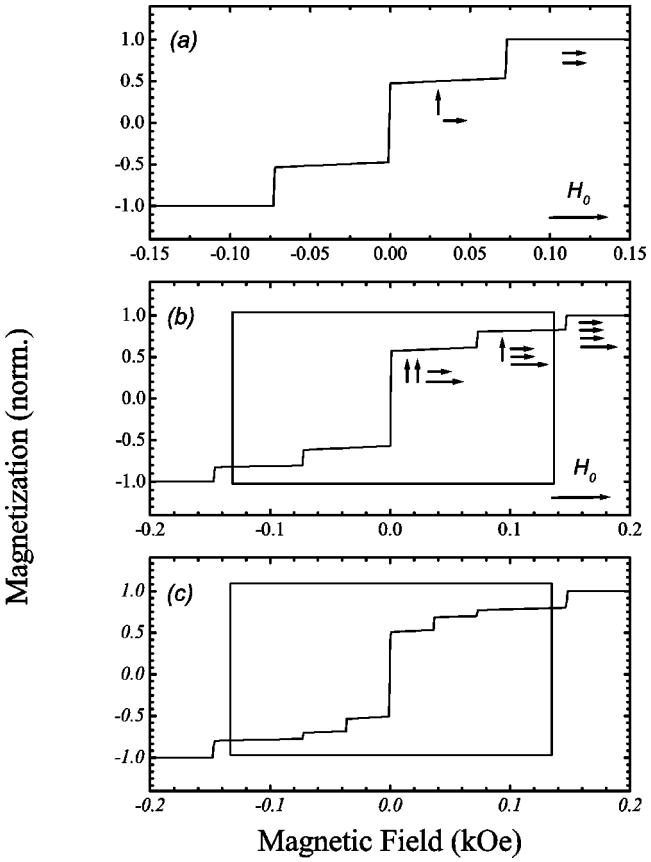


FIG. 4. Same as Fig. 3, but for $|H_{bq}|/|H_{bl}|=1.0$, corresponding to a realistic sample whose Cr thickness is about 25 Å.

exchange coupling: (i) the first one with $H_{bl}=-1.0$ kOe and $H_{bq}=0.1$ kOe. It lies in the region of the first antiferromagnetic peak of the bilinear exchange coupling, corresponding to a realistic sample whose Cr thickness is about 10 Å; (ii) the second set with $H_{bl}=-0.035$ kOe and $H_{bq}=0.035$ kOe. It is in the region of the second antiferromagnetic peak of the bilinear exchange coupling, corresponding to a realistic sample whose Cr thickness is about 25 Å.

### A. Fibonacci magnetic multilayers

The magnetization curves for the first set of parameters of the Fibonacci magnetic multilayers are shown in Fig. 3. For the third generation (which corresponds to the well known Fe/Cr/Fe trilayer), in the low field region, the magnetizations are antiparallel. As the field increases, they continuously rotate toward the field direction (second order phase transition) and the saturation is reached when the external magnetic field $H\sim1.91$ kOe. For the fifth generation there are two first order phase transitions at $H\sim0.71$ kOe and $H\sim0.87$ kOe, respectively. The saturation is reached at $H\sim2.93$ kOe. For the seventh generation, there are three first order phase transitions at $H\sim0.28$ kOe, $H\sim0.96$ kOe and $H\sim1.06$ kOe, respectively. The saturation is reached at $H\sim3.03$ kOe. For this set of parameters the majority of the transitions are of second order. Note that due to the different Fe layer thickness, for the fifth and seventh generations, the magnetization is not zero even for zero magnetic field. In Fig. 4 we show the results for the second set of parameters. For the third generation, due to the strong biquadratic field, there is no antiparallel phase in the low field region. Two magnetic phases are present: 90° ($H<72$ Oe) and saturated ($H>72$ Oe). The fifth generation presents three magnetic phases: (i) 90° ($H<72$ Oe); (ii) almost saturated (72 Oe $<H<0.14$ kOe); and (iii) saturated ($H>0.14$ kOe). The seventh generation presents four magnetic phases from 90° ($H<36$ Oe) to the saturated regime ($H>0.14$ kOe). All transitions are of first order. Note the striking self-similar pattern shown by the magnetization profile in this figure (see the windows).

### B. Double period magnetic multilayers

Figures 5(a) and 5(b) show our results for the double period magnetic multilayers, considering the first set of parameters. For the second generation, due to the double Fe layer, the magnetization has about 1/3 of its saturation value for zero magnetic field. There is a first order phase transition from antiparallel to an asymmetric phase at $H\sim0.69$ kOe. In this phase, the magnetizations are asymmetrically oriented along the magnetic field. When $H\sim1.34$ kOe the saturated phase emerges. For the fourth generation, for zero magnetic field, the magnetization has about 10% of its saturation value due to the different thickness of the Fe layers. There is a first order phase transition at $H\sim0.29$ kOe and the saturation is

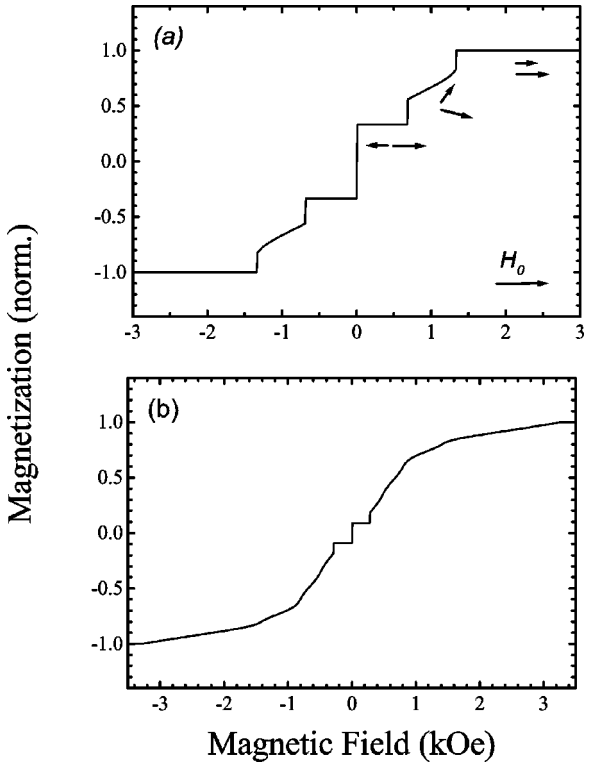


FIG. 5. Magnetization vs applied field for the second (a) and fourth (b) double period generations with $|H_{bq}|/|H_{bl}|=0.10$. The cubic anisotropy effective field is again $H_{ca}=0.5$ kOe. The Cr thickness is 10 Å.

reached at $H\sim 3.27$ kOe. All other phase transitions are of second order. For the second set of parameters (see Fig. 6), on the contrary, all transitions are of first order. For this set of parameters, there is no antiparallel phase in the low field region, due to the strong biquadratic field. For the second generation, the magnetization is about 2/3 of its saturation value when $H=0$. There are two magnetic phases: (i) 90° ($0<H<72$ Oe) and (ii) saturated ($H>72$ Oe). For the fourth generation, the magnetization for zero magnetic field is about 1/2 of its saturation value. Four magnetic phases are present, from the 90° ($0<H<38$ Oe) to the saturated phase ($H>0.14$ kOe). As in the Fibonacci case, a self-similar pattern is also present in the magnetization curves (see the window).

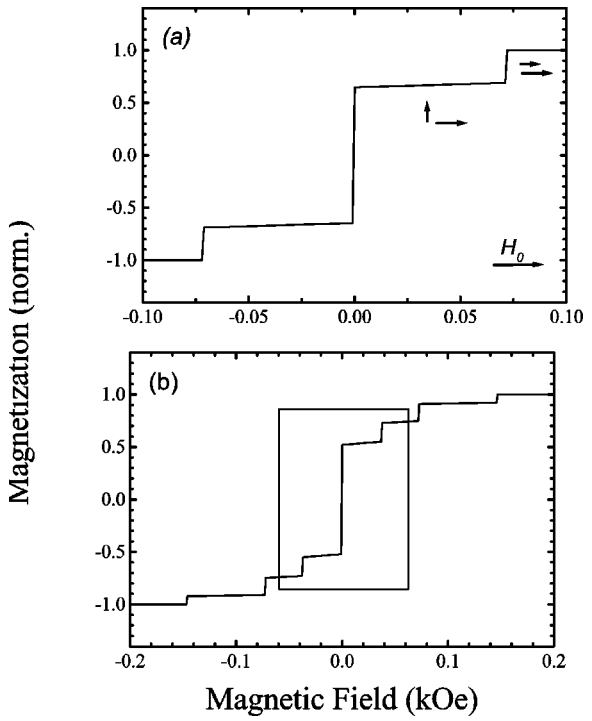


FIG. 6. Same as Fig. 5, but for $|H_{bq}|/|H_{bl}|=1.0$, corresponding to a realistic sample whose Cr thickness is about 25 Å.

## VI. CONCLUSIONS

We have studied quasiperiodic magnetic multilayers, composed by ferromagnetic Fe layers separated by nonmagnetic Cr layers, arranged according to the Fibonacci and double period quasiperiodic sequences. We consider that the Fe layers are linked by bilinear and biquadratic exchange couplings through Cr layers and present cubic anisotropy. The external magnetic field is applied in the plane of the layers and along an easy axis. We have used two numerical methods to determine the equilibrium configurations of the layers's magnetizations. The magnetization curves of these artificial structures were calculated considering two sets of experimental parameters recently reported.[6–8] Our results show that quasiperiodic magnetic multilayers exhibit a rich variety of configurations induced by the external magnetic field. In particular two points may be emphasized: (i) the effect of different thickness of Fe layers and (ii) the effect of the biquadratic exchange coupling.

The effect of different thickness of Fe layers is evident in the low field region. In that region, due to these differences, there is a net magnetization even if the alignment is antiparallel and the external magnetic field is zero. Besides, the nature of the phase transitions are changed by the different thickness [Fig. 3(a) shows only second order phase transitions, while Fig. 5(a) presents an additional first order phase transition]. These results suggest that, varying the thickness of Fe layers, it is possible to tailor magnetic multilayers to present desired specific phase transitions and critical fields. However, as the thickness of Fe layers increases, the crystalline anisotropy of Fe (100) films on Cr (100) also increases. Fortunately, as a characteristic of the quasiperiodic multilayers arrangements considered here, the maximum number of joint Fe layers is two (for the Fibonacci case) and three (for the double period case), no matter the value of their generation numbers. Besides, from a thickness greater than 40 Å, the crystalline anisotropy reaches saturation.[7]

On the other hand, the biquadratic exchange coupling plays a remarkable role in the features of the magnetization curves. For example, when the bilinear exchange coupling prevails, the majority of the transitions are of second order character (see Figs. 3 and 5). However, when the biquadratic exchange is compared to the bilinear one, in the presence of a stronger crystalline anisotropy,[8] the transitions are characterized by discontinuous jumps in the magnetization that indicate first order phase transitions. This can be considered as the basic signature of the biquadratic exchange coupling (see Figs. 4 and 6), although for the case where there is no biquadratic term, a first order phase transition appears due to the

anisotropy.[24] Furthermore, as shown by the windows in these figures, the magnetization curves of higher generations reproduce the magnetization curves of lower generations. This self-similar behavior is a general characteristic of quasiperiodic systems, although it is not present when the bilinear exchange prevails (Figs. 3 and 5). A possible explanation for these different behaviors is because the biquadratic exchange coupling induces long range correlations that emphasize the quasiperiodicity of the system. These long range correlations make the whole structure *seeing* its quasiperiodicity, which is reflected in the magnetization curves. This argument is reinforced by previous works on the correlation lengths of magnetic systems presenting biquadratic exchange coupling (see, for example, Sørensen and Young[25]).

The most appropriate experimental technique for studying the magnetization curves of magnetic films is the magneto-optical Kerr effect (MOKE).[8] However, because the MOKE measurements provide surface sensitivity on the scale of the optical penetration depth ($\sim$10 Å), it is necessary to use also a superconductor quantum interface device magnetometry.[19] The two techniques prove complementary in understanding the switching behavior of the multilayer films, as far as the magnetization curves are concerned. We hope that the present results can stimulate experimental studies of these structures.

## ACKNOWLEDGMENTS

The authors would like to thank the Brazilian Research Council CNPq for financial support and CESUP-RS where part of the numerical calculation was done.

[1] P. Grünberg, R. Schreiber, Y. Pang, M. O. Brodsky, and H. Sowers, Phys. Rev. Lett. **57**, 2442 (1986).
[2] M. N. Baibich, J. M. Broto, A. Fert, F. Nguyen Van Dau, F. Petroff, P. Etienne, G. Creuzet, A. Friederich, and J. Chazelas, Phys. Rev. Lett. **61**, 2472 (1988).
[3] W. J. Gallagher *et al.*, J. Appl. Phys. **81**, 3741 (1997).
[4] S. S. P. Parkin, N. More, and K. P. Roche, Phys. Rev. Lett. **64**, 2304 (1990).
[5] M. Ruhrig, R. Schafer, A. Hubert, R. Mosler, J. A. Wolf, S. Demokritov, and P. Grünberg, Phys. Status Solidi A **125**, 635 (1991).
[6] A. Azevedo, C. Chesman, S. M. Rezende, F. M. de Aguiar, X. Bian, and S. S. P. Parkin, Phys. Rev. Lett. **76**, 4837 (1996).
[7] S. M. Rezende, C. Chesman, M. A. Lucena, A. Azevedo, F. M. de Aguiar, and S. S. P. Parkin, J. Appl. Phys. **84**, 958 (1998).
[8] C. Chesman, M. A. Lucena, M. C. de Moura, A. Azevedo, F. M. de Aguiar, and S. M. Rezende, Phys. Rev. B **58**, 101 (1998).
[9] D. Shechtman, I. Blech, D. Gratias, and J. W. Cahn, Phys. Rev. Lett. **53**, 1951 (1984).
[10] P. J. Steinhardt and S. Ostlund, *The Physics of Quasicrystals* (World Scientific, Singapore, 1987).
[11] M. S. Vasconcelos, E. L. Albuquerque, and A. M. Mariz, J. Phys.: Condens. Matter **10**, 5839 (1998).
[12] M. Quilichini and T. Janssen, Rev. Mod. Phys. **69**, 277 (1997).
[13] P. M. C. de Oliveira, E. L. Albuquerque, and A. M. Mariz, Physica A **227**, 206 (1996).
[14] M. S. Vasconcelos and E. L. Albuquerque, Phys. Rev. B **57**, 2826 (1998).
[15] C. G. Bezerra and E. L. Albuquerque, Physica A **245**, 379 (1997); **255**, 285 (1998).
[16] M. Kohmoto, B. Sutherland, and K. Iguchi, Phys. Rev. Lett. **58**, 2436 (1987); M. Kohmoto, B. Sutherland, and C. Tang, Phys. Rev. B **35**, 1020 (1987).
[17] C. G. Bezerra, E. L. Albuquerque, and E. Nogueira, Jr., Physica A **267**, 124 (1999); M. S. Vasconcelos, E. L. Albuquerque and E. Nogueira, Jr. , *ibid.* **268**, 165 (1999).
[18] C. G. Bezerra, J. M. de Araújo, C. Chesman, and E. L. Albuquerque, Phys. Rev. B **60**, 9264 (1999).
[19] R. W. Wang, D. L. Mills, E. E. Fullerton, J. E. Matson, and S. D. Bader, Phys. Rev. Lett. **72**, 920 (1994).
[20] L. Turban, P. E. Berche, and A. B. Berche, J. Phys. A **27**, 6349 (1994).
[21] *Handbook of Global Optimization*, edited by R. Horst and P. M. Darlos (Kluwer, Dordrecht, 1995).
[22] S. Kirkpatrick, C. D. Geddat, Jr., and M. P. Vecchi, Science **220**, 671 (1983).
[23] W. H. Press, S. A. Teukolski, W. T. Vetterling, and B. P. Flanery, *Numerical Recipes* (Cambridge University Press, New York, 1998).
[24] W. Folkerts and S. T. Purcell, J. Magn. Magn. Mater. **111**, 306 (1992).
[25] E. S. Sørensen and A. P. Young, Phys. Rev. B **42**, 754 (1990).